

Forward kinematics modeling of spatial parallel linkage mechanisms based on constraint equations and the numerical solving method

Liyang Gao and Weiguo Wu*

School of Mechatronics Engineering, Harbin Institute of Technology, Heilongjiang, Harbin, P. R. China

(Accepted May 23, 2015. First published online: June 19, 2015)

SUMMARY

In order to solve general kinematics modeling problems and numerical stability problems of numerical methods for spatial parallel linkage mechanisms, a general modeling method and its numerical solving algorithm is proposed. According to the need for avoiding direct singular configurations, valid joint variable space and valid forward kinematics solutions (VKSs) are defined. Taking numerical convergence near singular points into account, the pseudo-arc length homotopy continuation algorithm is given to solve the kinematics model. Finally as an example, the joint variable space of the general Stewart platform mechanism is analyzed, which is proved to be divided into subspaces by direct singular surfaces. And then, forward kinematics solutions of 200 testing points are solved separately using the pseudo-arc length homotopy continuation algorithm, the Newton homotopy continuation algorithm and the Newton–Raphson algorithm (NRA). Comparison of the results shows that the proposed method is convergent to the same solution branch with the initial configuration on all the testing points, while the other two algorithms skip to other solution branches on some near singular testing points.

KEYWORDS: Spatial parallel linkage mechanism; Forward kinematics; Numerical solutions; Direct singularity; Homotopy continuation method.

1. Introduction

Scholars have conducted a significant amount of research regarding the kinematics problem for parallel mechanisms. The methods used can be divided into three categories, which are analytical methods, numerical methods, and methods of sensor installation. The closed-form expression of the kinematics problem for parallel mechanisms can be solved by using analytical methods, among which the Sylvester resultant method is the most common. An approach was given that can solve all 40 solutions of the forward kinematics problem for the Stewart platform by using a 13-order Sylvester resultant constructed by Gröbner basis.¹ Xiguang Huang reduced the order of the Sylvester resultant to 10 and simplified the complexity of the solution.² Analytical solutions of the kinematics problems for other parallel mechanisms are also derived by scholars,^{3–5} which are not enumerated here. Existing analytical methods of solving the forward kinematics problem for parallel mechanisms will generally result in a 20-order equation, which leads to complex computation. Because different mechanisms need to be re-derived, the application of the analytical method is limited. The method of sensor installation needs to install additional sensors (e.g., angle displacement sensor, line displacement sensor and so on) on some passive joints, which leads to inconveniences in practical applications.

Numerical methods are the approach to get the position and orientation of the moving platform within the scope of numerical accuracy by a kinematics model and the active joint variable values of the mechanism. With improvements in computation, numerical methods have more and more usages in parallel mechanism kinematics displacement analysis. The optimization methods, the

* Corresponding author. E-mail: wuwg@hit.edu.cn

Newton–Raphson method and other new intelligent methods are commonly used in the numerical method approach. An optimization method was given to solve numerical kinematics solutions for a 6–3–3 parallel robot by establishing a kinematics model with inverse kinematics equations and by using the squared residuals as the optimization object.⁶ Moreover, the kinematics model of a Stewart platform was solved by the Newton–Raphson method.^{7,8} However, all these numerical methods need an initial guess good enough to get convergence.

To obtain an approximation for forward kinematics equations, multilayer BP networks were trained by making inverse kinematics solutions as training samples.^{9,10} Approximations of the forward kinematics model of an ankle parallel mechanism was obtained by the fuzzy inference system, and a good approximation was achieved by applying the modified genetic algorithm to the model.¹¹ Also, Antonio Morell obtained the approximations of the forward kinematics models of parallel mechanisms by support vector regression.¹² These numerical approximation methods can be used in real time control and has a certain degree of versatility. But, they generally cause a problem of uneven distributed approximation error, which can lead to large approximation error in some areas when the model is convergent by the RMS error. Wang and Chen gave a generally applicable numerical method for the forward kinematics problem for parallel mechanisms, which assumed that each kinematics chain drove a moving platform independently and solved the kinematics solutions by using a coordinate rotation method to make all the moving platforms overlap.¹³ But this method has a complicated kinematics modeling process, which limits its application.

The homotopy continuation method in solving the forward kinematics solution of parallel mechanisms was proposed early on by scholars. All of the 40 forward kinematics solutions of the Stewart platform were obtained by using the Newton homotopy continuation method.¹⁴ And, the computation complexity of this method was reduced by using a homogeneous homotopy continuation method.¹⁵ By using the homotopy continuation method, Varedi obtained all the 16 kinematics solutions of the three-UPU mechanism.¹⁶ These studies are focused on getting all of the forward kinematics solutions of parallel mechanisms, rather than tracking certain branches of the forward kinematics solutions. There are more studies similar to the above literatures, however they are not mentioned here.

Most of the existing numerical methods do not consider the effect of the singularity of the mechanisms to the stability of the numerical algorithms. Also, the existing numerical methods cannot tell which solution among multiple solutions can be achieved in real applications. That is, if the joint variable vectors of the mechanisms correspond to multiple forward kinematics solutions, the existing numerical method cannot guarantee to be convergent to the solution of the same branch with the initial configuration on the configurations that are nearly singular. And, the skip between the forward kinematics solution branches may cause the discontinuous trajectory of the moving platform. In addition, the current versatile methods are complex for building the forward kinematics models and are not suitable for mechanized solutions. So, by analyzing the constraint equations of the kinematics pairs that consist of parallel mechanisms, a general kinematics modeling method for the spatial parallel linkage mechanisms is proposed and a numerical solving method based on the pseudo-arc length homotopy continuation method is proposed. These proposed methods guarantee the theoretical convergence on any nonsingular configurations, especially configurations near singular.

2. Establishment of Constraint Equations

The spatial parallel linkage mechanisms can be regarded as links connected by lower pairs and these lower pairs create the link movements under certain constraints. The mechanism kinematics models can be established if the equations of all the introduced constraints are found.

Some research has been conducted regarding the establishment of constraint equations for lower pairs. Javier Garcia de Jalón and Miguel Angel Serna classified constraint equations of the lower kinematics pairs in the planar mechanisms into two categories:¹⁷ the constant distance between two points and the constant area of triangles formed by three points. But, constraint equations deduced by Javier Garcia de Jalón do not fit for spatial mechanisms. Constraint equations of 3D joints were established by Sugiyama¹⁸ and Masarati.¹⁹ Sugiyama considered the situation of flexible mechanisms and orientation representations rather than only positions which were used in Masarati's deduction. However, these two methods are too complex in the kinematics modeling process for the lower pairs.

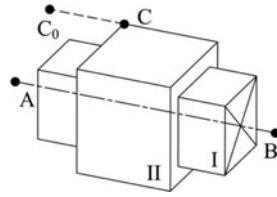


Fig. 1. Mechanism of the prismatic pair.

So, the 3D constraint equations of lower pairs are deduced here first, and then the method to establish a set of equations for the whole mechanism is given.

2.1. Establishment of the constraint equations for the lower pairs

The most generally used kinematics pairs for the spatial parallel linkage mechanisms are rotational pairs (R), prismatic pairs (P), cylindrical pairs (C), helical pairs (H), spherical pairs (S) and universal pairs (U). Among them, the active kinematics pairs are always the rotational pairs and the prismatic pairs. Because a universal pair can be regarded as a connection of two rotational pairs and a planar pair can be regarded as a connection of two prismatic pairs and a rotational pair, these two situations are ignored. The constraints of kinematic pairs are the holonomic constraints, so here they can be represented by position equations of pivot points fixed with linkages.

Because the constraint equations of each kinematics pair have similar derivation processes, we only show the derivation process of the prismatic pair constraint equations. The mechanism of the prismatic pair is shown in Fig. 1, where linkage I is defined as the rail of the prismatic pair and linkage II as the slider. Points A, B and C₀ are fixed to the rail and point C is fixed to the slider. Among them, points A and B are located on the axis of the rail and point C₀ is located on the initial position of point C.

Point C is limited to linear movement by the prismatic pair, so that line AB is parallel with line CC₀. Thus, the constraint equation is

$$(P_C - P_{C_0}) \times e = 0.$$

Where, P_C and P_{C_0} are the position vectors of points C and C₀ in the base coordinate system, respectively. And, if not mentioned separately, we will always use P_A , P_B , P_C and P_{C_0} to represent the position vectors of the pivot points A, B, C and C₀ in the base coordinate system, respectively. e is the unit vector of the rail axis and can be calculated by the following equation.

$$e = (P_A - P_B) / \|P_A - P_B\|. \tag{1}$$

When the prismatic pair is an active pair and assuming x is the joint variable, we can get the following constraint equation:

$$P_C - P_{C_0} = xe.$$

Table I shows constraint equations of all the involved lower pairs. Because special actuators like the three degrees-of-freedom (DOF) motor have already been designed, constraint equations of all the lower pairs involved are also given in Table I when they are active pairs. The pivot points chosen for other kinematics pairs in Table I are similar to the pivot points described for the prismatic pair. Among them, points A and B are points on the axis of linkage I and fixed with linkage I; point C is an arbitrary point fix with the linkage II; and, point C₀ is located on the initial position of point C and is fixed with linkage I. In Table I, θ , θ_r , θ_p , θ_y , and x are joint variables, which are the angle displacements or linear displacements of the joints; R_{rpy} is the rotational transformation matrix with the roll, pitch, yaw angle as θ_r , θ_p , θ_y respectively. R is the 3 × 3 rotational transformation matrix with the rotational angle θ around the axis of the kinematics pair and is written as Eq. (2); and P_h is the lead of the helical pair.

$$R = (1 - \cos \theta) ee^T + (\sin \theta) e \times I + (\cos \theta) I. \tag{2}$$

When establishing the constraint equations for the mechanisms, except for the above constraint equations of the kinematics pairs we also need equations for the rigid body constraint, which represents a mathematical relationship between the positions of the pivot points fixed in a rigid body. Based on the definition of a rigid body, the rigid body constraint equations of n ($n = 3, 4, 5 \dots$) pivot points are established in the following form to avoid formula singularity and extraneous roots.

$$\left\{ \begin{array}{l} \text{Collinear \& } n \geq 3 \rightarrow \left\{ \begin{array}{l} \|P_1 - P_2\| = E_1 \\ P_3 = E_2 P_1 + E_3 P_2 \\ \vdots \\ P_n = E_{2n-4} P_1 + E_{2n-3} P_2 \end{array} \right. \\ \\ \text{Coplanar \& } n \geq 4 \rightarrow \left\{ \begin{array}{l} \|P_1 - P_2\| = E_1 \\ \|P_2 - P_3\| = E_2 \\ \|P_3 - P_1\| = E_3 \\ P_4 = E_4 P_1 + E_5 P_2 + E_6 P_3 \\ \vdots \\ P_n = E_{3n-8} P_1 + E_{3n-7} P_2 + E_{3n-6} P_3 \end{array} \right. \\ \\ \text{O.W.} \rightarrow \left\{ \begin{array}{l} \left. \left\{ \begin{array}{l} \|P_1 - P_2\| = E_1 \\ \|P_2 - P_3\| = E_2 \\ \|P_3 - P_4\| = E_3 \end{array} \right\} \right\} n = 3 \\ \left. \left\{ \begin{array}{l} \|P_4 - P_1\| = E_4 \\ P_5 = E_5 P_1 + E_6 P_2 + E_7 P_3 + E_8 P_4 \\ \vdots \\ P_n = E_{4n-9} P_1 + E_{4n-10} P_2 + E_{4n-11} P_3 + E_{4n-12} P_4 \end{array} \right\} \right\} n = 4 \\ \left. \left\{ \begin{array}{l} \vdots \\ P_n = E_{4n-9} P_1 + E_{4n-10} P_2 + E_{4n-11} P_3 + E_{4n-12} P_4 \end{array} \right\} \right\} n \geq 5 \end{array} \right. \quad (3)$$

Where P_i ($i = 1, 2, \dots, n$) is the position vector of the i th pivot point and E_j ($j = 1, 2, \dots, 4n - 12$) is the constant determined by the mechanism parameters.

2.2. Establishment of the constraint equations of the whole mechanism

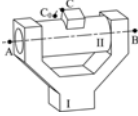

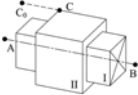
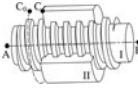
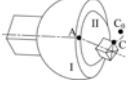
The constraint equations establishment method for the spatial parallel linkage mechanisms is given in this section. Because the parallel mechanisms always have multiple kinematics chains and the moving platform connects with all the kinematics chains, the process of the constraint equations establishment is to combine the constraint equations of the kinematics pairs sequentially from the base platform to the end of each of the kinematics chains and then to add the constraint equations formed by the moving platform.

Referring to the constraint equations in Table I, rules of combining constraint equations can be established as follows:

- (1) For adjacent kinematics pairs in each kinematics chain, linkage II of the moving-platform-near pair is defined to be linkage I of the base-platform-near pair and the pivot point C of the base-platform-near pair is sequentially defined as located on the pivot points A, B, and C_0 of the moving-platform-near pair to obtain the constraint equations.
- (2) Linkage I of the pair connected with the base platform linkage is defined as the base platform linkage and the positions of the pivot points A, B, and C_0 are known.

In order to get the constraint equations of the moving platform, three non-collinear pivot points are first needed to be chosen on the moving platform. Then, the pivot point C of all the kinematics pairs connected with the moving platform are created as to be located on the three chosen points, separately. All the constraint equations of the moving platform can be listed based on the constraint

Table I. Constraint equations of all the involved lower pairs.

Name of the kinematics pairs	mechanism	Non-active pairs constraint equations	Active pairs constraint equations
Rotational pair		$\ P_A - P_C\ = \ P_A - P_{C0}\ $ $\ P_B - P_C\ = \ P_B - P_{C0}\ $	$P_C - P_B = R(P_{C0} - P_B)$
Cylindrical pair		$\ (P_A - P_C) \times e\ = \ (P_A - P_{C0}) \times e\ $	$P_C - P_B = R(P_{C0} - P_B) + xe$
Prismatic pair		$(P_C - P_{C0}) \times e = 0$	$P_C - P_{C0} = xe$
Helical pair		$\theta = \frac{(P_C - P_{C0}) \cdot e}{P_h}$ $P_C - P_B = R(P_{C0} - P_B) + \frac{\theta P_h}{2\pi} e$	$P_C - P_B = R(P_{C0} - P_B) + \frac{\theta P_h}{2\pi} e$
Spherical pair		$\ P_A - P_C\ = \ P_A - P_{C0}\ $	$P_C - P_A = R_{ipy}(P_{C0} - P_A)$

equations shown in Table I. Then, a check for the existence of any n pivot points in a rigid body needs to be conducted. If they exist, constraint equations between these pivot points need to be replaced by the rigid body constraint equations given above. Finally, a process of simplification, such as eliminating the same equations and then directly solving the equations with only one unknown variable, is conducted. The flowchart from the above steps for establishing the mechanism constraint equations is shown in the Fig. 2.

By the method described above, the set of equations containing the position of the three fixed pivot points on the moving platform and other pivot points are established. Because solving the position and orientation of the moving platform by the given position of the three points on it is easy, solving the forward kinematics of the mechanisms is equal to that of solving the established equations. Though many new unknown variables in the kinematics model other than the variables that represent the position and orientation of the moving platform are introduced, the established constraint equations will be a 1 or 2 order polynomial equation, if there is no passive helical pair in the mechanism. In this case, the nonlinear degree of the model will be significantly lower than the model obtained by other methods, which can improve the speed of solving the equations.

3. Singularity Analysis of Mechanisms

Singularity of parallel mechanisms was defined by multiple scholars almost simultaneously in the early 1990s. Ma and Angeles classified the parallel mechanism singularities into architectural singularity, configuration singularity and formulation singularity by the formation reason of singularities and dimensions of a singular workspace.^{20,21} Gosselin defined the singularities of parallel mechanisms by the singularities of the coefficient matrix of the differential kinematics equations.²² Tsai named these three categories of singularities by inverse, direct (forward) and combined singularities in 1999.²³ Direct singularity makes the mechanism unable to bear the load along the singular DOF, while inverse singularity leads to movement incapacity of the moving platform in the singular DOF. Combined singularity is a situation where the above two singularities take place simultaneously. Sometimes, inverse singularity is used to obtain stiffness enhancement of mechanisms in a certain direction and direct singularity may lead to uncertain movement of the moving platform. So, in general singularity of a parallel mechanism means direct singularity. First, direct singularity criterion based on the

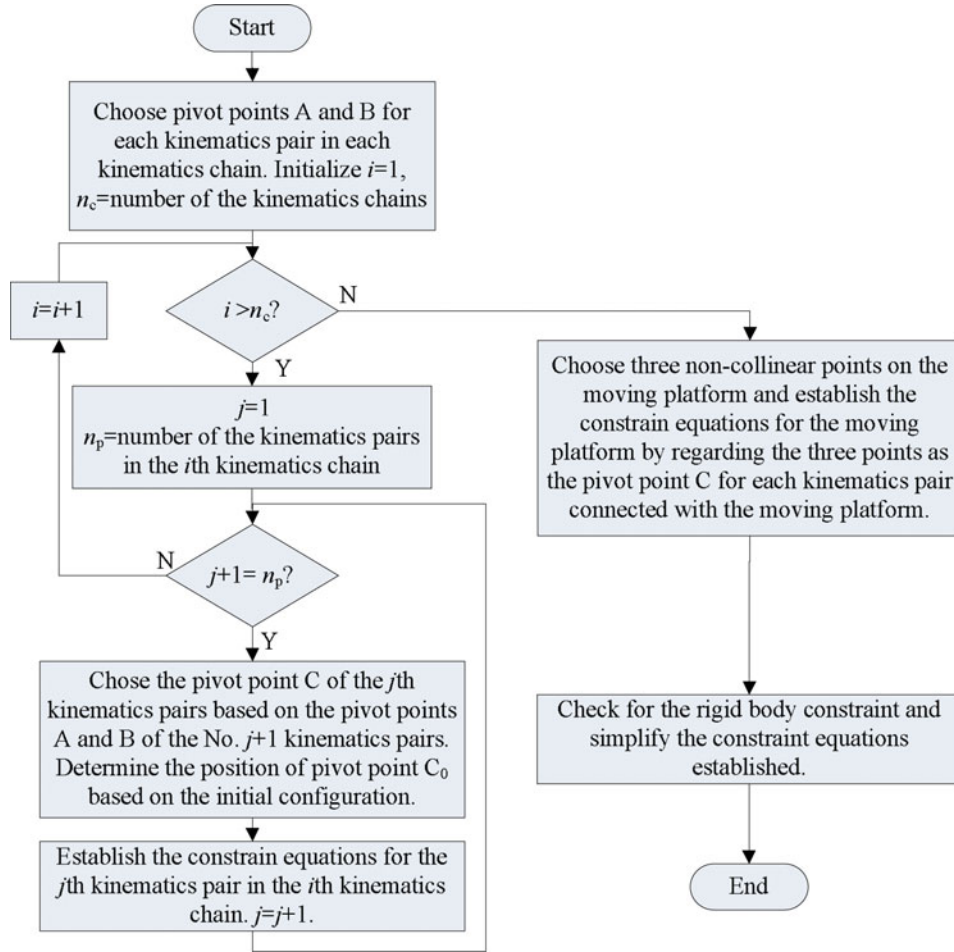


Fig. 2. Flowchart of the establishment of the mechanism constraint equations.

constraint equations established in the former section is shown, and then the valid joint variable space is defined.

Assume that the established constraint equations can be written as follows:

$$F(v, x) = [F_1(v, x) \ \cdots \ F_n(v, x)]^T = 0. \tag{4}$$

Where F is an n dimension polynomials column vector, v is an n dimension unknown column vector whose elements are the position coordinates values of the pivot points, and x is an m dimension joint variable column vector. Thus the differential kinematics equation be written as Eq. (5).

$$B\dot{v} = A\dot{x}. \tag{5}$$

Where A and B have the form of:

$$A = \begin{bmatrix} -\partial F_1/\partial x_1 & \cdots & -\partial F_1/\partial x_m \\ \vdots & & \vdots \\ -\partial F_n/\partial x_1 & \cdots & -\partial F_n/\partial x_m \end{bmatrix} \quad B = \begin{bmatrix} \partial F_1/\partial v_1 & \cdots & \partial F_1/\partial v_n \\ \vdots & \ddots & \vdots \\ \partial F_n/\partial v_1 & \cdots & \partial F_n/\partial v_n \end{bmatrix}.$$

According to the definition of direct singularity of parallel mechanisms, $\det(B) = 0$ is the criterion of direct singular configuration. Generally, workspace of the parallel mechanisms is segmented into subspaces by “surfaces” consisting of singular points. But, it is much more complicated for the joint space of parallel mechanisms. Some mechanisms with multiple forward kinematic solutions may

have different singular “surfaces” for each forward kinematics solution in the joint space (the 3-RRR mechanism, the 3-PRR mechanism and the 3-RPR mechanism for example). Based on this point, researchers studied the nonsingular transition between different forward kinematics solutions.^{24–26} To represent the joint space that can be reached in real works, the valid joint space (VJS) of a certain initial configuration is defined here based on the above mentioned phenomenon.

Definition 1. The VJS of a certain initial configuration is the direct nonsingular continuous subspace of the whole joint space that contains the initial configuration.

The configurations of mechanisms should not reach the direct singular configurations or even near the direct singular configurations, so the valid joint variable space is the joint variable space that can be actually reached in real works. Because the transition between different forward kinematics solutions is not used in most works, the following defined VKS can be regard as the only forward kinematics solution reached in real works in the VJS.

Definition 2. The VKS of a configuration is the forward kinematics solution in the VJS with the same branch as the initial configuration.

4. To Solve the Constraint Equations

An algorithm to solve the VKS and an error estimate method is explained here.

Existing numerical methods cannot theoretically guarantee to obtain the VKS and can only distinguish solutions by range restriction or other ways. To solve this problem, an algorithm that can theoretically solve the VKS is produced based on the homotopy continuation method. The homotopy continuation method is a kind of numerical method for nonlinear equations. The idea is to track a set of similar equations with known solutions, so as to get solutions of the equations to be solved by coefficient transition of the known solutions equations. In the use of the homotopy method to solve numerical solutions of forward kinematics problem for parallel mechanisms, Raghavan made the first efforts in 1991¹⁴ followed by Sreenivasan, who improved this method in 1992.¹⁵ But, their research was focused on solving all the solutions of the forward kinematics problem and do not consider the effect of the singularities on the convergence of the homotopy path. Thus these methods cannot directly solve the VKS. The pseudo-arc length homotopy continuation method used here can jump over singular points, so the VKS can be solved by tracking the homotopy path of the initial configuration. The homotopy function of the joint variable vector \mathbf{x}^* is constructed as follows to track the solution branch of the VKS.

$$\mathbf{H}(\mathbf{v}, \lambda) = \mathbf{F}(\mathbf{v}, \lambda \mathbf{x}^* + (1 - \lambda) \mathbf{x}_0) \quad \lambda \in [0, 1]. \quad (6)$$

There are $\mathbf{H}(\mathbf{v}_0, 0) = \mathbf{0}$ and $\mathbf{H}(\mathbf{v}^*, 1) = \mathbf{0}$, so when λ changes from 0 to 1, the solution of the equation $\mathbf{H} = \mathbf{0}$ changes from \mathbf{v}_0 to \mathbf{v}^* . According to the topological invariant of the homotopy method, \mathbf{v}^* is the VKS when the increment of λ is small enough. But when the VJS is not a convex space, there may be a λ that makes the mechanism reach or near to the singular points and the algorithm above cannot converge in that situation. Thus, the homotopy continuation method with the pseudo-arc length constraint²⁷ shown by Eq. (7) is used to guarantee the convergence.

$$\mathbf{D}(\mathbf{v}, \lambda, s) = \begin{bmatrix} \mathbf{H}(\mathbf{v}, \lambda) \\ N(\mathbf{v}, \lambda, s) \end{bmatrix}_{n+1 \times 1} = \mathbf{0}. \quad (7)$$

Where $N(\mathbf{v}, \lambda, s)$ is the pseudo-arc length constraint polynomial and can be written as (8)

$$N(\mathbf{v}, \lambda, s) = 0.5 \dot{\mathbf{v}}(s_0) \cdot \mathbf{v}(s) + 0.5 \dot{\lambda}(s_0) \lambda(s) - (s - s_0). \quad (8)$$

Where s is the coordinate of the pseudo-arc length and s_0 is the initial value of s , $[\dot{\mathbf{v}}(s) \dot{\lambda}(s)]^T$ is the tangent vector of the equations and can be calculated with Eq. (9).

$$\hat{\mathbf{D}}(\mathbf{v}(s_0), \lambda(s_0)) \begin{bmatrix} \dot{\mathbf{v}}(s_0) \\ \dot{\lambda}(s_0) \end{bmatrix} = \frac{\partial \mathbf{D}(\mathbf{v}, \lambda, s)}{\partial s} = \begin{bmatrix} \mathbf{0} \\ 1 \end{bmatrix}. \quad (9)$$

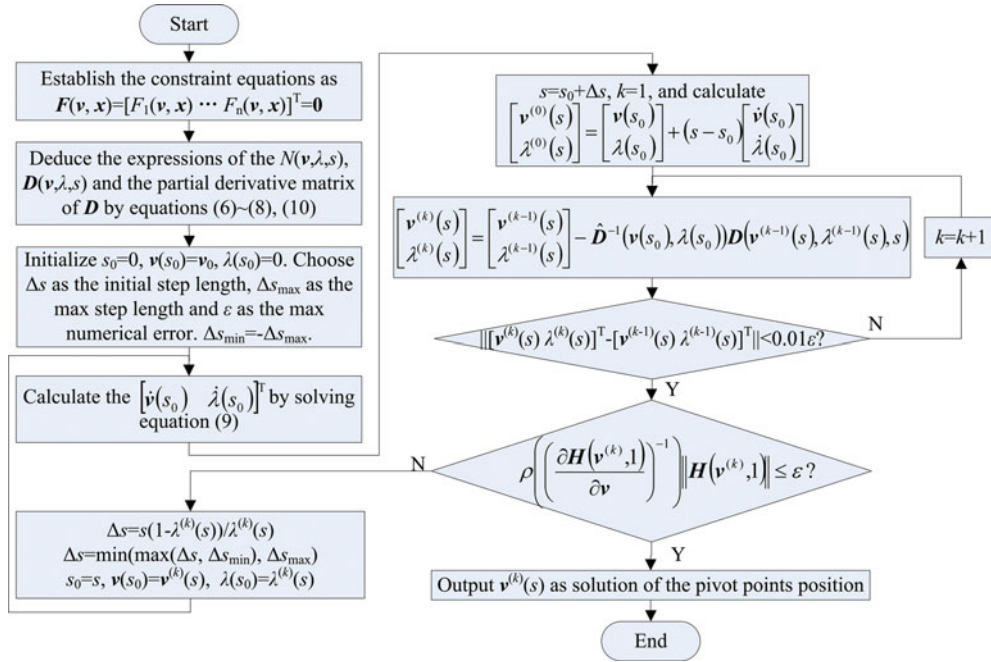


Fig. 3. The flowchart of the pseudo-arc length homotopy continuation algorithm.

Where \hat{D} is the partial derivative matrix of D on $[v, \lambda]^T$ and has the form as Eq. (10).

$$\hat{D}(v, \lambda) = \begin{bmatrix} \frac{\partial H(v, \lambda)}{\partial v} & \frac{\partial H(v, \lambda)}{\partial \lambda} \\ \frac{\partial N(v, \lambda, s)}{\partial v} & \frac{\partial N(v, \lambda, s)}{\partial \lambda} \end{bmatrix}_{\substack{n \times n & n \times 1 \\ 1 \times n & 1 \times 1}}_{n+1 \times n+1} \tag{10}$$

Formula (11) is the Newton secant method to solve $v(s)$ and $\lambda(s)$ with given $v(s_0)$ and $\lambda(s_0)$.

$$\begin{bmatrix} v^{(k)}(s) \\ \lambda^{(k)}(s) \end{bmatrix} = \begin{bmatrix} v^{(k-1)}(s) \\ \lambda^{(k-1)}(s) \end{bmatrix} - \hat{D}^{-1}(v(s_0), \lambda(s_0)) D(v^{(k-1)}(s), \lambda^{(k-1)}(s), s). \tag{11}$$

The initial iteration can be determined according to formula (12).

$$\begin{bmatrix} v^{(0)}(s) \\ \lambda^{(0)}(s) \end{bmatrix} = \begin{bmatrix} v(s_0) \\ \lambda(s_0) \end{bmatrix} + (s - s_0) \begin{bmatrix} \dot{v}(s_0) \\ \dot{\lambda}(s_0) \end{bmatrix}. \tag{12}$$

The error between the k th iteration results $v^{(k)}$ and v^* can be estimated by (13).

$$e^{(k)} = \|v^* - v^{(k)}\| \leq \rho \left(\left(\frac{\partial H(v^{(k)}, 1)}{\partial v} \right)^{-1} \right) \|H(v^{(k)}, 1)\| \leq \epsilon. \tag{13}$$

Where $\rho(\cdot)$ is the spectral radius operator and ϵ is the error tolerance. With error estimation, numerical solutions with arbitrary precision can be theoretically solved. Proved by Keller, this algorithm can skip the singular points and guarantee the convergence in the same branch,²⁸ which is not demonstrated here. The flowchart of the pseudo-arc length homotopy continuation algorithm to solve the kinematics problem for the spatial parallel linkage mechanisms is shown in Fig. 3.

Table II. Comparison of the three algorithms.

	The pseudo-arc length homotopy continuation algorithm	The Newton homotopy continuation algorithm	The NRA
Theoretical convergence on the near singular configurations	Yes	No	No
Dependence on the initial guess	No	No	Yes
Computational complexity	C_N^2	C_N^2	C_N
Orders of the partial derivative matrix	$n+1$	n	n

Shown in Fig. 3, the pseudo-arc length homotopy continuation algorithm needs to conduct the Newton secant algorithm for each iteration step of the pseudo-arc length variable s . Also, the Newton homotopy continuation algorithm needs to conduct the Newton secant algorithm for each iteration step of the homotopy variable λ . So, if the computational complexity of the NRA is assumed to be C_N , then the computational complexities of the pseudo-arc length and the Newton homotopy continuation algorithm are both C_N^2 . The comparison of the pseudo-arc length homotopy continuation algorithm, the Newton homotopy continuation algorithm and the NRA are shown in Table II.

In Table II, n is the equation number of the constraint equations. The computational complexities of the two homotopy continuation algorithms are both the square of the NRA computational complexity. And the order of the partial derivative matrix used by the pseudo-arc length homotopy continuation algorithm is one order higher than that in the other two algorithms. So, among the three compared algorithms, the computation time of the pseudo-arc length homotopy continuation algorithm is the longest and the NRA computational time is the shortest. But the pseudo-arc length homotopy continuation algorithm has the advantage of theoretical convergence for the near singular configurations and independence on the initial iteration value. These will be shown in the next section by the example of the Stewart platform.

5. Case Study of the Stewart Platform Mechanism

The forward kinematics problem of the Stewart platform mechanism (six-SPS) is solved in this section as an example to verify the proposed method. First, the kinematics model of the mechanism is established by the method given in Section 2 and the singularity analysis of the joint variable space is conducted. Then, the kinematics model is solved separately by using the pseudo-arc length homotopy continuation algorithm, the Newton homotopy continuation algorithm and the NRA. Finally, the results of the three methods are contrasted.

The mechanism of the Stewart platform is shown in Fig. 4. The centers of six spherical pairs on the base platform are asymmetric and as are the centers of six spherical pairs on the moving platform. The pivot points of the spherical pairs on the base platform are chosen, as described in Section 2, to be the centers of themselves as D_i (corresponding to point A in Table I), where $i = 1, 2, \dots, 6$ and hereinafter are the same. Similarly, pivot points of the prismatic pairs are chosen to be point D_i , E_i , and F_i (corresponding to point A, B, and C_0 , respectively in Table I) and the pivot points of the spherical pairs on the moving platform are chosen to be the centers of themselves as G_i (corresponding to point A, in Table I). The right-hand coordinate frame ΣD_3 -xyz shown in Fig. 4 is the base coordinate frame. The z-axis is vertically upward, and the x-axis extends from point D_3 to point D_2 . Another right-hand coordinate frame $\Sigma G_3 - x'y'z'$ is the coordinate frame fixed with the moving platform, and the x' -axis extends from point G_3 to point G_2 . Table III shows the position coordinate vector of the spherical pair centers on the base platform and the moving platform in their own local coordinate frame separately.

P_{D_i} and P_{G_i}' in Table III are the position coordinate vectors of point D_i in the base coordinate frame and the position coordinate vector of point G_i in the moving platform coordinate frame respectively. Notice that points D_i , E_i , and F_i are three collinear pivot points with rigid body constraints. The

Table III. Position coordinate vectors of the spherical pair centers.

Position vectors	Values (unit: mm)	Position vectors	Values (unit: mm)
P_{D1}	$[200.764, 53.795, 0]^T$	$P_{G1'}$	$[122.475, 122.475, 0]^T$
P_{D2}	$[169.706, 0, 0]^T$	$P_{G2'}$	$[51.764, 0, 0]^T$
P_{D3}	$[0, 0, 0]^T$	$P_{G3'}$	$[0, 0, 0]^T$
P_{D4}	$[-31.058, 53.795, 0]^T$	$P_{G4'}$	$[-70.711, 122.475, 0]^T$
P_{D5}	$[53.795, 200.764, 0]^T$	$P_{G5'}$	$[-44.829, 167.303, 0]^T$
P_{D6}	$[115.911, 200.764, 0]^T$	$P_{G6'}$	$[96.593, 167.303, 0]^T$

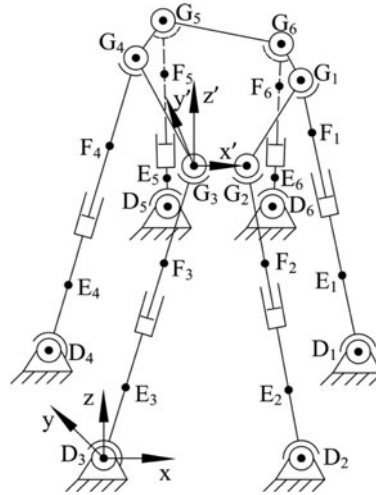


Fig. 4. Mechanism of the Stewart platform.

constraint equations of each SPS kinematics chain can be written as follows:

$$\begin{aligned}
 e &= (P_{Ei} - P_{Di}) / \|P_{Ei} - P_{Di}\| \\
 P_{Fi} &= \|P_{Fi} - P_{Di}\| e + P_{Di} \\
 P_{Gi} &= P_{Fi} + x_i e
 \end{aligned}
 \tag{14}$$

Where x_i is the joint variable of the prismatic pair in the i th kinematics chain. Formula (15) can be obtained by simplifying (14).

$$\|P_{Gi} - P_{Di}\|^2 = \left(\sqrt{\|P_{Fi} - P_{Di}\|^2} + x_i \right)^2 = L_i^2.
 \tag{15}$$

Where L_i is the length of the i th leg and is the input of the forward kinematics problem. Next, the constraint equations of the platform are established. $G_i (i = 1 \sim 6)$ are six coplanar pivot points with the rigid body constraints, so their constraint equations have the following form:

$$\begin{cases}
 P_{G2} = E_1 P_{G1} + E_2 P_{G3} + E_3 P_{G5} \\
 P_{G4} = E_4 P_{G1} + E_5 P_{G3} + E_6 P_{G5} \\
 P_{G6} = E_7 P_{G1} + E_8 P_{G3} + E_9 P_{G5} \\
 \|P_{G1} - P_{G3}\| = E_{10} \\
 \|P_{G3} - P_{G5}\| = E_{11} \\
 \|P_{G5} - P_{G1}\| = E_{12}
 \end{cases}
 \tag{16}$$

Where $E_j(j = 1 \sim 12)$ are constants determined by the position coordinate values shown in Table III. Among them the E_1, E_2, \dots, E_9 can be calculated by projecting the $\mathbf{P}_{G2}, \mathbf{P}_{G4}, \mathbf{P}_{G6}$ onto the basis vector set composed by $\mathbf{P}_{G1}, \mathbf{P}_{G3}, \mathbf{P}_{G5}$ as shown in the Eq. (17). E_{10}, E_{11}, E_{12} are actually the length of the segments G_1G_3, G_3G_5, G_5G_1 and can be calculated by Eq. (18).

$$\begin{bmatrix} E_1 & E_4 & E_7 \\ E_2 & E_5 & E_8 \\ E_3 & E_6 & E_9 \end{bmatrix} = ([\mathbf{P}'_{G1} \quad \mathbf{P}'_{G3} \quad \mathbf{P}'_{G5}] + \mathbf{M})^{-1} ([\mathbf{P}'_{G2} \quad \mathbf{P}'_{G4} \quad \mathbf{P}'_{G6}] + \mathbf{M}) \quad (17)$$

$$\begin{bmatrix} E_{10} \\ E_{11} \\ E_{12} \end{bmatrix} = \begin{bmatrix} \|\mathbf{P}'_{G1} - \mathbf{P}'_{G3}\| \\ \|\mathbf{P}'_{G3} - \mathbf{P}'_{G5}\| \\ \|\mathbf{P}'_{G5} - \mathbf{P}'_{G1}\| \end{bmatrix}. \quad (18)$$

\mathbf{M} is the 3×3 matrix where all the elements of it are 1 in Eq. (17). Table IV shows the results of E_1, E_2, \dots, E_{12} .

Constraint equations of the whole mechanism can be established as follows by integrating Eq. (15) and (16).

$$\mathbf{F}(\mathbf{v}, \mathbf{x}) = \begin{bmatrix} (x_{G1} - x_{D1})^2 + (y_{G1} - y_{D1})^2 + (z_{G1} - z_{D1})^2 - L_1^2 \\ (x_{G2} - x_{D2})^2 + (y_{G2} - y_{D2})^2 + (z_{G2} - z_{D2})^2 - L_2^2 \\ (x_{G3} - x_{D3})^2 + (y_{G3} - y_{D3})^2 + (z_{G3} - z_{D3})^2 - L_3^2 \\ (x_{G4} - x_{D4})^2 + (y_{G4} - y_{D4})^2 + (z_{G4} - z_{D4})^2 - L_4^2 \\ (x_{G5} - x_{D5})^2 + (y_{G5} - y_{D5})^2 + (z_{G5} - z_{D5})^2 - L_5^2 \\ (x_{G6} - x_{D6})^2 + (y_{G6} - y_{D6})^2 + (z_{G6} - z_{D6})^2 - L_6^2 \\ E_1x_{G1} + E_2x_{G3} + E_3x_{G5} - x_{G2} \\ E_1y_{G1} + E_2y_{G3} + E_3y_{G5} - y_{G2} \\ E_1z_{G1} + E_2z_{G3} + E_3z_{G5} - z_{G2} \\ E_4x_{G1} + E_5x_{G3} + E_6x_{G5} - x_{G4} \\ E_4y_{G1} + E_5y_{G3} + E_6y_{G5} - y_{G4} \\ E_4z_{G1} + E_5z_{G3} + E_6z_{G5} - z_{G4} \\ E_7x_{G1} + E_8x_{G3} + E_9x_{G5} - x_{G6} \\ E_7y_{G1} + E_8y_{G3} + E_9y_{G5} - y_{G6} \\ E_7z_{G1} + E_8z_{G3} + E_9z_{G5} - z_{G6} \\ (x_{G1} - x_{G3})^2 + (y_{G1} - y_{G3})^2 + (z_{G1} - z_{G3})^2 - E_{10} \\ (x_{G3} - x_{G5})^2 + (y_{G3} - y_{G5})^2 + (z_{G3} - z_{G5})^2 - E_{11} \\ (x_{G5} - x_{G1})^2 + (y_{G5} - y_{G1})^2 + (z_{G5} - z_{G1})^2 - E_{12} \end{bmatrix} = \mathbf{0} \quad (19)$$

Equation (19) is a set of equations that has 18 polynomial equations and a highest order of 2, where $\mathbf{v} = [x_{G1}x_{G2}x_{G3}x_{G4}x_{G5}x_{G6}y_{G1}y_{G2}y_{G3}y_{G4}y_{G5}y_{G6}z_{G1}z_{G2}z_{G3}z_{G4}z_{G5}z_{G6}]^T$ is the 18-dimensional vector of the unknowns and $\mathbf{x} = [L_1L_2L_3L_4L_5L_6]^T$ is the six-dimensional vector of the joint variables. Other symbols in Eq. (19) represent constants. Before the forward kinematics problem is solved, the singularity of the joint variable space is analyzed to show the VJS of a given initial configuration. Because the Jacobian matrix of the $\mathbf{F}(\mathbf{v}, \mathbf{x})$ is used in the singularity analysis, its expression is shown in Appendix A. There are six joint variables for the Stewart mechanism, so the whole joint variable space cannot be expressed in a Cartesian coordinate frame. At 190 (mm) the $L_1, L_3,$ and L_5 is fixed and the joint variable space spanned by $L_2, L_4,$ and L_6 using the traversal algorithm is

Table IV. Parameters in the constraint equations.

Parameter symbols	Parameter values	Parameter symbols	Parameter values
E_1	0.3333	E_7	0.9107
E_2	0.9107	E_8	-0.2440
E_3	-0.2440	E_9	0.3333
E_4	-0.2440	E_{10}	207.846
E_5	0.3333	E_{11}	207.846
E_6	0.9107	E_{12}	207.846

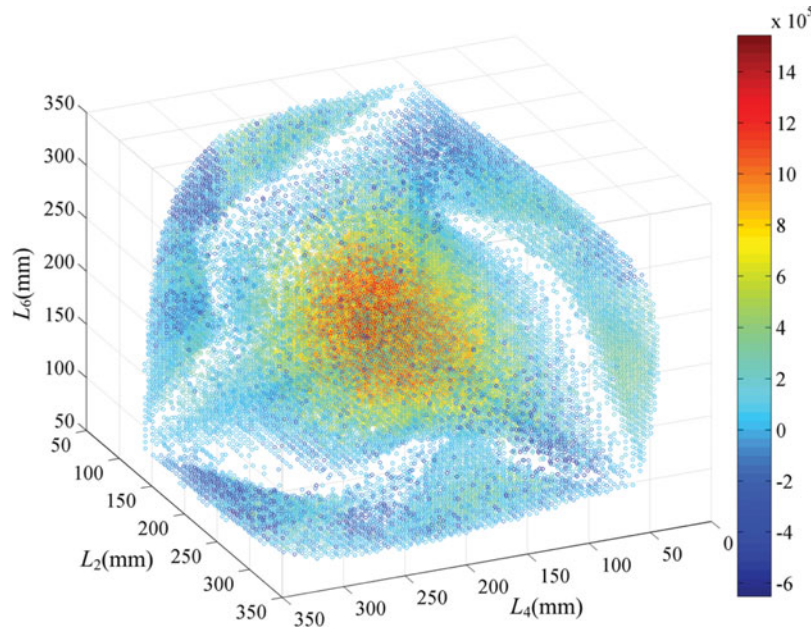


Fig. 5. Joint variable space of the Stewart platform mechanism.

analyzed. Figure 5 demonstrates the results of the joint variable space, in which the color of each point represents its Jacobian determinant. Points with a light blue color are the singular points.

To clearly display the results of the singularity analysis, Fig. 6 is used to show the near singular points (with a Jacobian determinant of less than 0.1% of the average value) in the plane where $L_6 = 190, 210, 230,$ and 250 (mm). It is revealed that the joint variable space is divided into subspaces by the surface consisting of singular points.

Demonstrated by Fig. 6, the large subspace that contains the initial joint variable vector $[170, 170, 170, 170, 170, 170]^T$ (mm) is chosen to be the VJS of the Stewart mechanism. By choosing points on the nonsingular paths from the initial configuration in the position and orientation space of the moving platform, pivot point position coordinate vectors (denoted by \mathbf{v}) and joint variable vectors (denoted by \mathbf{x}) for each \mathbf{v} (this process is shown in the Appendix B) are generated. Then, 100 normal points and 100 near singular points in the VJS are randomly chosen to calculate their VKS, whose pivot point position coordinate vectors and joint variable vectors are denoted by \mathbf{v}_i and \mathbf{x}_i ($i = 1 \dots 200$), respectively. The \mathbf{x}_i is the input of the forward kinematics analysis. The \mathbf{v}_i is the analytical solution of the forward kinematics problem for the Stewart mechanism and also the forward kinematics solution that can be reached from the initial configuration by the nonsingular path. The forward kinematics solutions of the 200 points are calculated separately by the pseudo-arc length homotopy continuation method, the Newton homotopy continuation method and the NRA, which are represented by \mathbf{v}_{PHi} , \mathbf{v}_{NH_i} and \mathbf{v}_{NR_i} ($i = 1 \dots 200$), respectively. The calculation is done in a PC computer with the Pentium Dual-Core E5700 CPU and the CPU frequency is 2.99 GHz. The numerical accuracy is chosen to be 0.0005 and the maximum iteration number is chosen to be 150. The relative error of the above results

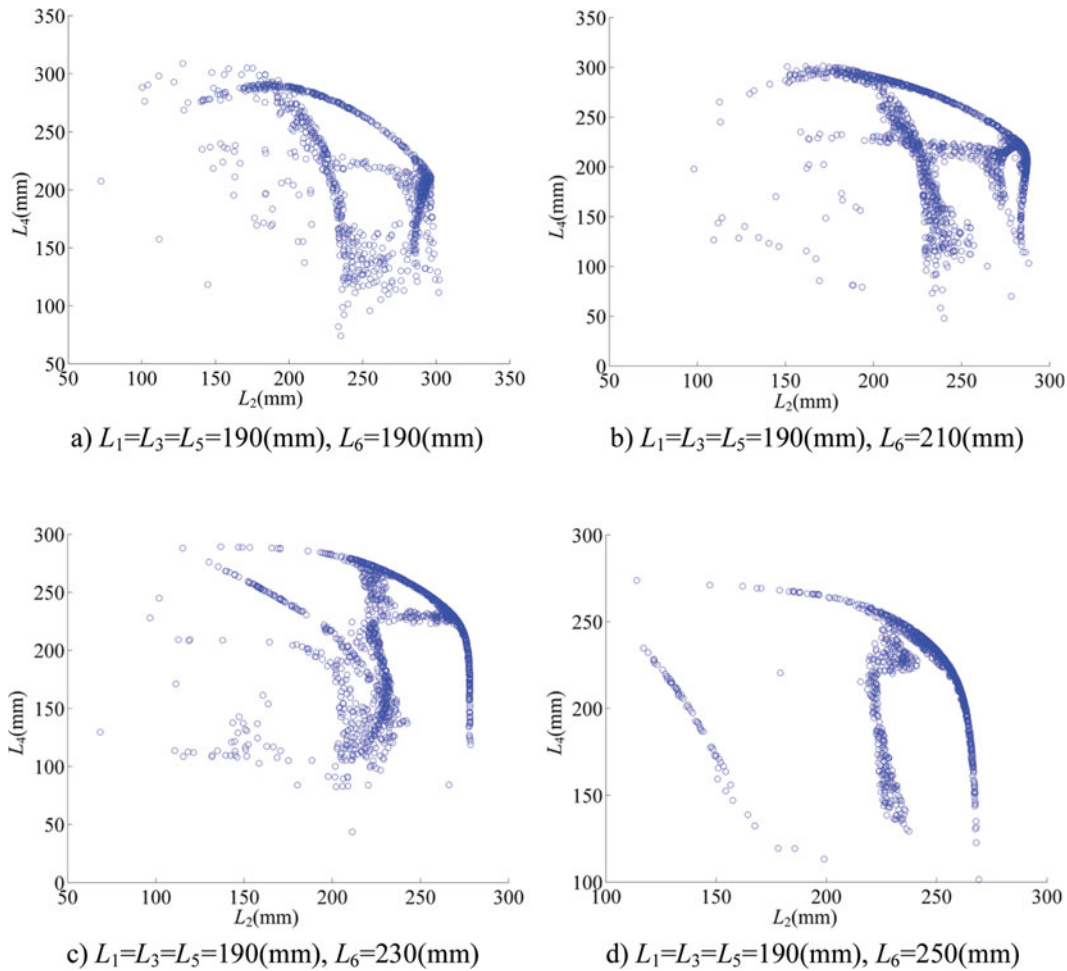


Fig. 6. Distribution of near singular points in the joint variable space. (a) $L_1 = L_3 = L_5 = 190(\text{mm}), L_6 = 190(\text{mm})$ (b) $L_1 = L_3 = L_5 = 190(\text{mm}), L_6 = 210(\text{mm})$. (c) $L_1 = L_3 = L_5 = 190(\text{mm}), L_6 = 230(\text{mm})$ (d) $L_1 = L_3 = L_5 = 190(\text{mm}), L_6 = 250(\text{mm})$.

is defined as:

$$\begin{aligned}
 e_{PHi} &= \|\mathbf{v}_i - \mathbf{v}_{PHi}\| / \|\mathbf{v}_i\| \\
 e_{NH i} &= \|\mathbf{v}_i - \mathbf{v}_{NH i}\| / \|\mathbf{v}_i\| \quad (i = 1 \sim 200) \\
 e_{NR i} &= \|\mathbf{v}_i - \mathbf{v}_{NR i}\| / \|\mathbf{v}_i\|
 \end{aligned}
 \tag{20}$$

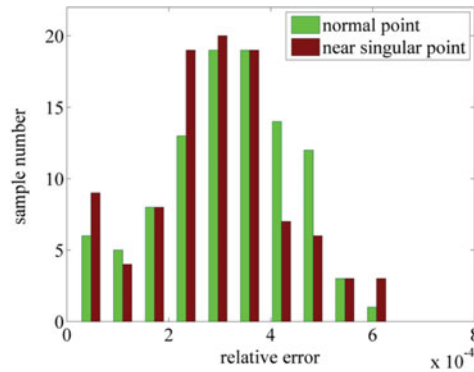
Figure 7 is the relative error distraction of the results.

For the nonsingular points, the relative errors of the three algorithms are all below 0.1%. But for the near singular points, the pseudo-arc length homotopy continuation method can obtain solutions that have the same precision as with the nonsingular points, while the Newton homotopy continuation method and the NRA get solutions with large differences as compared to the analytical solutions. Verified by the inverse kinematics (shown in Appendix B), these solutions with large differences to the analytical solutions are also solutions for the forward kinematics problem and are solutions of another branch, so that the Newton homotopy continuation method and the NRA are not convergent to the same solution branch with the initial configuration on these points. The comparison of the calculation results is shown in Table V.

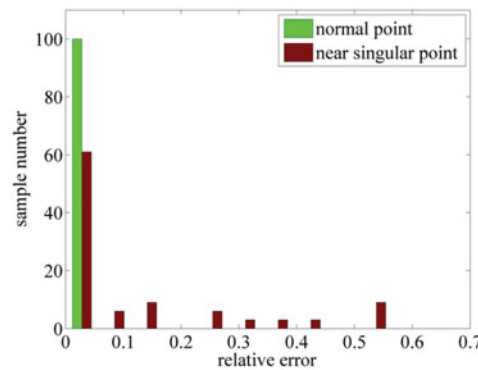
Based on the data in Table V, though the proposed algorithm needs more computational time compared to the Newton homotopy continuation algorithm and the NRA, it can converge to the same solution branch with the initial configuration on all the testing points. Because the Newton homotopy continuation algorithm also tracks the solution branch of the initial configuration by the variation of λ but cannot guarantee to be convergent, performance of it is much better than that of NRA, which is

Table V. Comparison of the calculation results of the three algorithms.

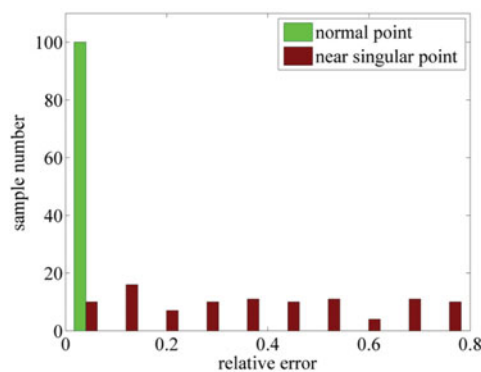
	The pseudo-arc length homotopy continuation algorithm	The newton homotopy continuation algorithm	The NRA
Ratio of points with relative error less than 0.1% in the near singular points	100%	61%	10%
Average relative error of the normal points result	0.026%	0.024%	0.036%
Average computational time for one point (sec)	3.203	2.286	0.208



a) Relative error of the pseudo-arc length homotopy continuation method results



b) Relative error of the Newton homotopy continuation method results



c) Relative error of the NRA results

Fig. 7. Relative error distraction of the three algorithms. (a) Relative error of the pseudo-arc length homotopy continuation method results. (b) Relative error of the Newton homotopy continuation method results. (c) Relative error of the NRA results.

the most effective in the aspect of computational time. However, the Newton homotopy continuation algorithm and the NRA skip to other solution branches on 39% and 90% near singular testing points, respectively. This may lead to a discontinued trajectory in the motion of the moving platform.

6. Conclusions

- (1) A general method to establish the kinematics models for the special linkage mechanisms is proposed by combining the constraint equations of lower pairs.
- (2) A general method for solving VKS is proposed by combining the pseudo-arc length homotopy continuation algorithm and the established kinematics model. Convergence advantage of the algorithm on near singular points is verified by solving the forward kinematics problem of the general Stewart platform mechanism and comparing the results of the proposed algorithm with the results of the Newton homotopy continuation algorithm and the NRA.

Appendix A. The Jacobian matrix of $F(\mathbf{v}, \mathbf{x})$

The Jacobian matrix \mathbf{J} of the $F(\mathbf{v}, \mathbf{x})$ shown in the Eq. (19) is the partial derivative matrix $\partial F(\mathbf{v}, \mathbf{x})/\partial \mathbf{v}$. Because the Jacobian matrix is an 18×18 sparse matrix, it is displayed by giving expressions of all its nonzero elements in the Table A1.

In Table A1, the element symbol $J_{ij}(i, j = 1, 2, 3...18)$ represents the matrix element of \mathbf{J} in the i th row and the j th column.

Appendix B. The inverse kinematics verification of the forward kinematics solutions

The position and orientation parameters of the moving platform can be denoted as $\theta_r, \theta_p, \theta_y, x, y, z$, among which the $\theta_r, \theta_p, \theta_y$ are the Euler angles of the moving platform coordinate frame relative to the base coordinate frame in the 3–2–1 order. And the x, y, z are the position coordinate values of the origin of the moving platform coordinate frame in the base coordinate frame. So $\mathbf{u} = [\theta_r, \theta_p, \theta_y, x, y, z]^T$ can be used as the position and orientation parameter vector of the moving platform and the position and orientation space is \mathbf{R}^6 . The pivot point position coordinate vector \mathbf{v} can be calculated by the following equation.

$$\mathbf{v} = \mathbf{T}(\mathbf{u}) \left[\mathbf{P}'_{G1}^T \quad \mathbf{P}'_{G2}^T \quad \mathbf{P}'_{G3}^T \quad \mathbf{P}'_{G4}^T \quad \mathbf{P}'_{G5}^T \quad \mathbf{P}'_{G6}^T \right]^T. \tag{A1}$$

In Eq. (A1), $\mathbf{T}(\mathbf{u})$ is the transformation matrix of the moving platform coordinate frame relative to the base coordinate frame, and can be calculated by Eq. (A2).

$$\mathbf{T}(\mathbf{u}) = \begin{bmatrix} c_p c_r & s_p c_r s_y - c_y s_r & s_p c_r c_y + s_y s_r & x \\ c_p s_r & s_p s_r s_y + c_y s_r & s_p s_r c_y - s_y c_r & y \\ -s_p & c_p s_y & c_p c_y & z \\ 0 & 0 & 0 & 1 \end{bmatrix}. \tag{A2}$$

In Eq. (A2), the c_j and $s_j(j = r, p, y)$ represent $\cos(\theta_j)$ and $\sin(\theta_j)$ respectively. By solving the kinematics model $F(\mathbf{v}, \mathbf{x}) = 0$, the forward kinematics solution of the analyzed Stewart mechanism can be written as $\mathbf{v}(\mathbf{x})$. When $\mathbf{v}(\mathbf{x})$ is the forward kinematics solution corresponding to the input joint variable vector \mathbf{x} , the condition Eq. (A3) holds, which has the form of the inverse kinematics solution

Table A1. Nonzero elements of the Jacobian matrix of the $F(\mathbf{v}, \mathbf{x})$.

Element symbol	Expression	Element symbol	Expression	Element symbol	Expression	Element symbol	Expression
$J_{1,1}$	$2(x_{G1} - x_{D1})$	$J_{1,7}$	$2(y_{G1} - y_{D1})$	$J_{1,13}$	$2(z_{G1} - z_{D1})$	$J_{2,2}$	$2(x_{G2} - x_{D2})$
$J_{2,8}$	$2(y_{G2} - y_{D2})$	$J_{2,14}$	$2(z_{G2} - z_{D2})$	$J_{3,3}$	$2(x_{G3} - x_{D3})$	$J_{3,9}$	$2(y_{G3} - y_{D3})$
$J_{3,15}$	$2(z_{G3} - z_{D3})$	$J_{4,4}$	$2(x_{G4} - x_{D4})$	$J_{4,10}$	$2(y_{G4} - y_{D4})$	$J_{4,16}$	$2(z_{G4} - z_{D4})$
$J_{5,5}$	$2(x_{G5} - x_{D5})$	$J_{5,11}$	$2(y_{G5} - y_{D5})$	$J_{5,17}$	$2(z_{G5} - z_{D5})$	$J_{6,6}$	$2(x_{G6} - x_{D6})$
$J_{6,12}$	$2(y_{G6} - y_{D6})$	$J_{6,18}$	$2(z_{G6} - z_{D6})$	$J_{7,1}$	E_1	$J_{7,2}$	-1
$J_{7,3}$	E_2	$J_{7,5}$	E_3	$J_{8,7}$	E_1	$J_{8,8}$	-1
$J_{8,9}$	E_2	$J_{8,11}$	E_3	$J_{9,13}$	E_1	$J_{9,14}$	-1
$J_{9,15}$	E_2	$J_{9,17}$	E_3	$J_{10,1}$	E_4	$J_{10,3}$	E_5
$J_{10,4}$	-1	$J_{10,5}$	E_6	$J_{11,7}$	E_4	$J_{11,9}$	E_5
$J_{11,10}$	-1	$J_{11,11}$	E_6	$J_{12,13}$	E_4	$J_{12,15}$	E_5
$J_{12,16}$	-1	$J_{12,17}$	E_6	$J_{13,1}$	E_7	$J_{13,3}$	E_8
$J_{13,5}$	E_9	$J_{13,6}$	-1	$J_{14,7}$	E_7	$J_{14,9}$	E_8
$J_{14,11}$	E_9	$J_{14,12}$	-1	$J_{15,13}$	E_7	$J_{15,15}$	E_8
$J_{15,17}$	E_9	$J_{15,18}$	-1	$J_{16,1}$	$2(x_{G1} - x_{G3})$	$J_{16,3}$	$2(x_{G3} - x_{G1})$
$J_{16,7}$	$2(y_{G1} - y_{G3})$	$J_{16,9}$	$2(y_{G3} - y_{G1})$	$J_{16,13}$	$2(z_{G1} - z_{G3})$	$J_{16,15}$	$2(z_{G3} - z_{G1})$
$J_{17,3}$	$2(x_{G3} - x_{G5})$	$J_{17,5}$	$2(x_{G5} - x_{G3})$	$J_{17,9}$	$2(y_{G3} - y_{G5})$	$J_{17,11}$	$2(y_{G5} - y_{G3})$
$J_{17,15}$	$2(z_{G3} - z_{G5})$	$J_{17,17}$	$2(z_{G5} - z_{G3})$	$J_{18,1}$	$2(x_{G1} - x_{G5})$	$J_{18,5}$	$2(x_{G5} - x_{G1})$
$J_{18,7}$	$2(y_{G1} - y_{G5})$	$J_{18,11}$	$2(y_{G5} - y_{G1})$	$J_{18,13}$	$2(z_{G1} - z_{G5})$	$J_{18,17}$	$2(z_{G5} - z_{G1})$

of the Stewart mechanism.

$$\mathbf{x} = \begin{bmatrix} \sqrt{(x_{G1} - x_{D1})^2 + (y_{G1} - y_{D1})^2 + (z_{G1} - z_{D1})^2} \\ \sqrt{(x_{G2} - x_{D2})^2 + (y_{G2} - y_{D2})^2 + (z_{G2} - z_{D2})^2} \\ \sqrt{(x_{G3} - x_{D3})^2 + (y_{G3} - y_{D3})^2 + (z_{G3} - z_{D3})^2} \\ \sqrt{(x_{G4} - x_{D4})^2 + (y_{G4} - y_{D4})^2 + (z_{G4} - z_{D4})^2} \\ \sqrt{(x_{G5} - x_{D5})^2 + (y_{G5} - y_{D5})^2 + (z_{G5} - z_{D5})^2} \\ \sqrt{(x_{G6} - x_{D6})^2 + (y_{G6} - y_{D6})^2 + (z_{G6} - z_{D6})^2} \end{bmatrix}. \quad (\text{A3})$$

The \mathbf{v} and \mathbf{x} of an arbitrary \mathbf{u} can be generated by Eqs. (A1)~(A3), which are regarded as the theoretical solution and the input of the forward kinematics problem for the Stewart platform respectively.

References

1. D. Gan, Q. Liao, J. S. Dai *et al.*, "Forward displacement analysis of the general 6–6 Stewart mechanism using Gröbner bases," *Mech. Mach. Theory*, **44**(9), 1640–1647 (2009).
2. X. G. Huang, "A Study on some Issues for Kinematics of Mechanism and their Algebraic Methods [D]," (Beijing University of Posts and Telecommunications, Beijing, 2008).
3. M. S. Tsai, T. N. Shiau, Y. J. Tsai *et al.*, "Direct kinematic analysis of a 3-PRS parallel mechanism," *Mech. Mach. Theory*, **38**(1), 71–83 (2003).
4. D. Gan and S. Wei, "Forward Kinematics Analysis of the New 3-CCC Parallel Mechanism," *IEEE, International Conference on Mechatronics and Automation*, (2007) pp. 905–910.
5. Y. Lu, P. Wang, S. Zhao, B. Hu, J. Han and C. Sui, "Kinematics and statics analysis of a novel 5-DoF parallel manipulator with two composite rotational/linear active legs," *Robot. Comput.-Integr. Manuf.* **30**(1), 25–33 (2014).
6. H. Gao, "Research on Application and Theory of Mechanism for 6–3–3 Parallel Mechanism [D]," (Hefei University of Technology, Hefei, 2007).
7. C. Yang, Q. Huang, P. O. Ogbobe *et al.*, "Forward Kinematics Analysis of Parallel Robots using Global Newton–Raphson Method," *IEEE, Intelligent Computation Technology and Automation*, (2009), vol. 3, pp. 407–410.
8. F. Liu, X. Zhang, Y. Wei and H. Wu, "The Forward Kinematics Analysis of 6-UPS Parallel Mechanism based on Newton Iteration," *Machinery Design & Manufacture*, (2013) (5), pp. 173–176.

9. M. Dehghani, M. Ahmadi, A. Khayatian *et al.*, “Neural Network Solution for Forward Kinematics Problem of HEXA Parallel Robot,” *IEEE, American Control Conference*, (2008) pp. 4214–4219.
10. P. J. Parikh and S. S. Y. Lam, “A hybrid strategy to solve the forward kinematics problem in parallel manipulators,” *IEEE Trans. Robot.* **21**(1), 18–25 (2005).
11. P. K. Jamwal, S. Q. Xie, Y. H. Tsoi and K. C. Aw, “Forward kinematics modelling of a parallel ankle rehabilitation robot using modified fuzzy inference,” *Mech. Mach. Theory*, **45**(11), 1537–1554 (2010).
12. A. Morell, M. Tarokh and L. Acosta, “Solving the forward kinematics problem in parallel robots using support vector regression,” *Eng. Appl. Artif. Intell.* **26**(7), 1698–1706 (2013).
13. L. C. T. Wang and C. C. Chen, “On the numerical kinematic analysis of general parallel robotic manipulators,” *IEEE Trans. Robot. Autom.* **9**(3), 272–285 (1993).
14. M. Raghavan, “The Stewart Platform of General Geometry has 40 Configurations,” *ASME Design and Automation Conference*, Chicago, IL, (1991), vol. 32(2), pp. 397–402.
15. S. V. Sreenivasan and P. Nanua, “Solution of the Direct Position Kinematics Problem of the General Stewart Platform using Advanced Polynomial Continuation,” *22nd Biennial Mechanisms Conference*, Scottsdale, AZ, (1992) pp. 99–106.
16. S. M. Varedi, H. M. Daniali and D. D. Ganji, “Kinematics of an offset 3-UPU translational parallel manipulator by the homotopy continuation method,” *Nonlinear Anal.: Real World Appl.* **10**(3), 1767–1774 (2009).
17. J. G. de Jalón, M. A. Serna and R. Avilés, “Computer method for kinematic analysis of lower-pair mechanisms—II position problems,” *Mech. Mach. Theory*, **16**(5), 557–566 (1981), ISSN 0094-114X.
18. H. Sugiyama, J. L. Escalona and A. A. Shabana, “Formulation of three-dimensional joint constraints using the absolute nodal coordinates,” *Nonlinear Dyn.* **21**(2), 167–195 (2003), ISSN 0924-090X.
19. P. Masarati, “A formulation of kinematic constraints imposed by kinematic pairs using relative pose in vector form,” *Multibody Syst. Dyn.* **29**(2), 119–137 (2013), ISSN 1384-5640.
20. O. Ma and J. Angeles, “Architecture singularities of platform manipulators,” *IEEE, International Conference on Robotics and Automation*, (1991) pp. 1542–1547.
21. O. Ma and J. Angeles, “Architecture singularities of parallel manipulators,” *Int. J. Robot. Autom.* **7**(1), 23–29 (1992).
22. C. Gosselin and J. Angeles, “Singularity analysis of closed-loop kinematic chains,” *IEEE Trans. Robot. Autom.* **6**(3), 281–290 (1990).
23. L. W. Tsai, “*Robot Analysis: The Mechanics of Serial and Parallel Manipulators* (John Wiley & Sons, Hoboken, New Jersey, USA, 1999).
24. E. Macho, O. Altuzarra, V. Petuya and A. Hernandez, “Workspace enlargement merging assembly modes. Application to the 3-RRR planar platform,” *Int. J. Mech. Control*, **10**(1), 13–20 (2009).
25. E. Macho, V. Petuya, O. Altuzarra and A. Hernandez, “Planning nonsingular transitions between solutions of the direct kinematic problem from the joint space,” *J. Mech. Robot.* **4**(4), 041005–1–041005–9 (2012); doi:10.1115/1.4007306.
26. H. Bamberger, A. Wolf and M. Shoham, “Assembly mode changing in parallel mechanisms,” *IEEE Trans. Robot.* **24**(4), 765–772 (2008). doi: 10.1109/TRO.2008.926863.
27. H. B. Keller, “Numerical Solution of Bifurcation and Nonlinear Eigenvalue Problems,” *Applications of Bifurcation Theory*, (1977), pp. 359–384.
28. H. B. Keller, “Constructive Methods for Bifurcation and Nonlinear Eigenvalue Problems,” *Computing Methods in Applied Sciences and Engineering, I*. (Berlin Heidelberg, Springer, 1979) pp. 241–251.